https://doi.org/10.2352/issn.2169-2629.2021.29.123

Estimation of BRDF Measurements for Printed Colour Samples

Tanzima Habib, Phil Green and Peter Nussbaum, Norwegian University of Science and Technology, Gjøvik, Norway

Abstract

In this paper, we describe a method to estimate BRDF measurements for different printed colours, using just the BRDF measurements of the substrate and the primary inks. A model is trained using the BRDF measurements of the unprinted substrate and the cyan, magenta, and yellow inks, where four different diffuse and specular measurements of each are used as predictors to find the reflectance factor at a different lighting and viewing angle. In this approach only four spectral measurements of each test colour are required to estimate BRDF. This reduces the number of measurements required to estimate BRDF of a printed surface and to estimate the spectral reflectances that describe its material surface characteristics.

Introduction

Obtaining the bidirectional reflectance distribution function (BRDF) for a material surface is essential in modelling surface appearance. To measure BRDF we need to know the position on the surface, the direction of the incident light, the direction of the reflection and the amount of light that is reflected. BRDF is measured over a hemisphere where the incident light angle and reflection angle changes direction parameterized by the azimuth angle and the zenith angle, making it a somewhat tedious and time-consuming process.

There are many ways to measure BRDF, including, a gonio-reflectometer, a dome-shaped system and image based BRDF measurements. A gonio-reflectometer illuminates the flat target and detects the reflectance using a sensor over a hemisphere around the target. This method of measuring BRDF is very precise with high angular resolution but also very time consuming [1-2]. The second type uses multiple detectors and light sources that are installed on a dome shaped frame and the full BRDF can be captured at once without moving any component [3-4]. A drawback of this system is that its installation requires many detectors and light sources which is expensive, and this also makes the system bulky as the size increases with the increase in resolution [3]. However, Ben-Ezra et al. has demonstrated that a smaller dome shaped system can be created by using light emitting diodes that both act as emitters and detectors. To avoid time consuming processes and high cost, much research has been done to acquire BRDF measurements using an image-based system where a digital camera, a light source and a spherical sample are used [5-8]. But an image-based system does not give us spectral data, which provides more information about the material characteristics.

Now if we need to measure BRDF for printed samples we will have to measure each colour patch. We make use of the ink mixing model for a print dataset such that using the BRDF measurements of the substrate and the primaries we can estimate the BRDF of other ink combinations.

In this paper, we present a BRDF measurement estimation method that addresses the requirement to reduce the number of measurements in order to model BRDF for a particular printer and substrate. These measurements then can be used to optimize a BRDF model and obtain BRDF parameters to reproduce surface appearance of a particular printed surface.

In earlier work [9-10], we showed how a BRDF workflow is possible within an ICC profile using iccMAX and, given a tristimulus value obtained using 45º:0º measurement geometry, how we can estimate the BRDF parameters for that ink combination and substrate. For this work BRDF parameters are estimated by optimizing a BRDF model based on BRDF measurements. Estimating the BRDF measurements will simplify the process of implementing the BRDF workflow described.

Method

In this section, we discuss the method used to estimate BRDF measurements.

BRDF Measurements

The BRDF of seventeen printed samples on glossy paper were measured. The range of these reflectances is 380nm to 780nm, in steps of 5nm. A GON 360 goniometer equipped with CAS 140CT array spectrophotometer was used, and the BRDF at reflection angles from -30° to 65° in intervals of 5° were measured for five incidence angles 0°, -15°, -30°, -45° and -60°. Figure 1 shows the training set for BRDF measurement estimation. Samples chosen were the substrate, cyan, magenta, and yellow. Figure 2 shows the thirteen test samples whose BRDF were measured for evaluation.

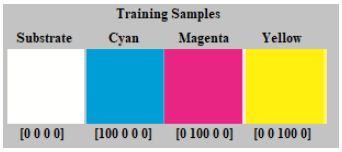

Figure 1. Visual representation of the substrate and the primaries cyan, magenta, and yellow that forms the training set.

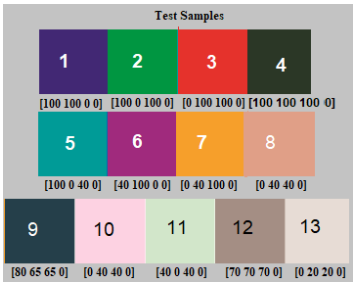

Figure 2. Visual representation of the thirteen test samples whose BRDF were measured.

Observations

Figure 3 and 4 shows the plots of reflectance factors obtained for incidence angle -60° and incidence angle -45° respectively with reflection angles -30° to 65° in steps of 5°, excluding the specular peak of the substrate and cyan sample respectively. The specular

reflections are primarily the illumination of the source spectral power distribution. Diffuse reflection at 0°:45° measurement geometry is the color of material. The intermediate angles combine both diffuse and specular reflections. The dominating diffuse reflections have spectral shape similar to the spectral shape of 0°:45° measurement. While the two reflectances at the adjacent reflection angles to the specular peak i.e., reflection angles 5° away from the specular peaks have dominating specular reflection, which can be seen in figure 3 and 4, and have reflectance factors relative to a perfect diffuser that are greater than1. This is also seen for measurements at other incidence angles. It is also observed that among the dominating diffuse reflection spectra, the spectrum with the highest reflectance factors has a small degree of influence of specular reflection and thus changes its spectral shape slightly from the diffuse spectra. These spectra are with reflection angles 10° away from the specular peak. Thus, as the measurements move away from the specular peak the influence of specular reflection reduces. This helps us to separate the modelling of specular reflection from the rest and to select the predictor reflectances from the training set accordingly. Therefore, we decided to model spectra with dominating diffuse reflection and the near-to-specular reflection using the same predictor reflectances.

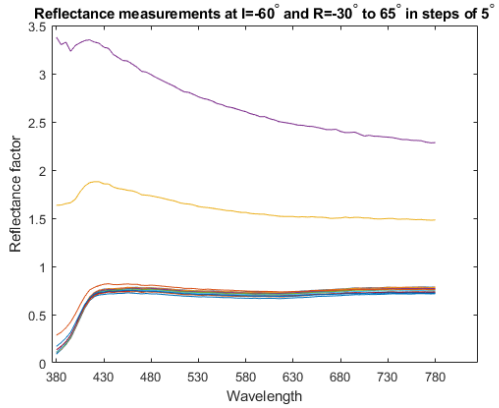

Figure 3. BRDF measurement plot of the substrate for incidence angle -60° and reflection angles -30° to 65° in steps of 5° excluding the specular peak.

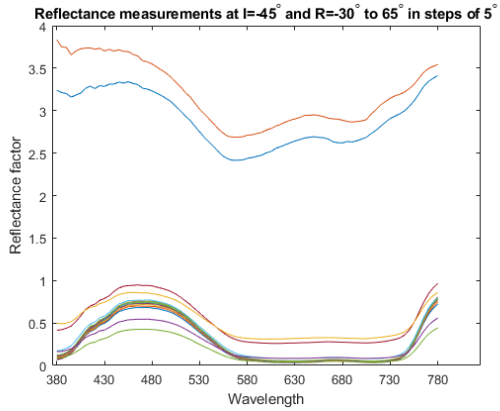

Figure 4. BRDF measurement plot of cyan for incidence angle -45° and reflection angles -30° to 65° in steps of 5° excluding the specular peak.

Estimation Method

A third-order polynomial regression was used to estimate the BRDF measurement. A regression model was created for each combination of incidence angle and reflection angle. In this case, we have 5 incidence angles and 20 reflection angles forming a total of 100 combinations. When the reflection angle is close to the incidence angle of light, the detector occludes some light and the reflectance cannot be measured. In figure 5, the grey patches and the patches enclosed by black squares are the shadowed areas. These sets of incidence and reflection angles combination were not modeled because of this shadowing. Also, those combinations of angles for which measurement data were missing were not used for modelling. This finally gives us 91 combinations of incidence and reflection angles for which we can create the estimation models.

The predictor set comprises of two base reflectances of the substrate (*xw1*,*xw2*), cyan (*xc1*,*xc2*), magenta (*xm1*,*xm2*) and yellow (*xy1*,*xy2*) samples chosen at a particular set of (incidence angle, reflection angle) e.g.: (-45º, 0º) and (-60º,65º). These reflectances are each of size 1x81 and are combined as shown in equation 1, to form the predictor matrix *X*.

$$X = \begin{pmatrix} xw1' & xw2' \\ xc1' & xc2' \\ xm1' & xm2' \\ xy1' & xy2' \end{pmatrix} \quad (1)$$

The response vector *Y* in equation 2 is the combination of training reflectances of *yw*, *yc*, *ym* and *yy* measured at (incidence angle, reflection angle) for which we are creating the estimation model. Once the model is created, for prediction we require the two defined base reflectances of the test samples. Using the same two base reflectances of a test sample we can predict the reflectances at any other combination of incidence and reflection angles using its corresponding estimation model.

$$Y = \begin{pmatrix} yw' \\ yc' \\ ym' \\ yy' \end{pmatrix} \quad (2)$$

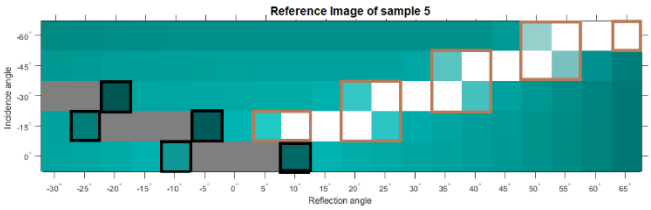

Figure 5. sRGB representation of the BRDF measurements of test sample 5 with incidence angles on the y-axis and reflection angles on the x-axis.

In figure 5, the white patches outside the brown squares are the specular peaks where incidence angle = -reflection angle. At these specular angles the reflectance spectra are predominantly the illumination spectra. The patches marked by the brown squares have a mix of specular reflection and diffuse reflection. As the area nears to the specular peak the specular reflection dominates diffuse reflection. We call these mixes near-to-specular reflections. The rest have dominating diffuse reflection.

Thus, while modelling, the two bases chosen for specular reflection, are (-45º,45º) midrange specular reflection and (-60º,60º) highest specular reflection for the training and test data. For patches with diffuse reflection and near-to-specular reflection are modelled with the same two bases, one at (-45º,0º) and another at (-60º,65º) the lightest patch of the training and test data that is not a specular peak. Therefore, to estimate BRDF measurements of a test sample, we will need in total of four measurements of that samples at (-45º,45º), (-60º,60º), (-45º,0º) and (-60º,65º). This reduces the requirement of measuring 100 reflectances per test sample to just 4.

Results and Discussion

For all the 13 test samples, the BRDF measurements have been estimated for five incidence angles and 20 reflection angles except for the shadowed and missing reflections. For all the estimated measurements, the normalized root mean square difference (NRMSD) was calculated relative to the reference measurements as shown in table 1. CIELAB based colour difference ΔE_{00} and colour difference ΔE_{IPT} in IPT colour space were calculated as shown in table 2 and 3 respectively. These colour difference models correspond to colour spaces that are designed for luminance levels from slightly above zero to that of a perfect diffuse white [11]. As the reflectance factors relative to the perfect diffuse reflector at near-to-specular peak go beyond 1 (i.e., they are brighter than a perfect diffuser), these colour difference models have a less defined relationship with perceived difference for these brighter colours. Colour difference in IPT colour space are said to be more perceptually uniform [12]. We show results for both ΔE_{00} and ΔE_{IPT} to illustrate the quality of prediction for these specular highlights. Figures 9-13 show how estimated luminance Y varies at every incidence angle and reflection angle combination compared to its reference. The results are discussed according to diffuse reflection, near-to-specular reflection and specular reflection sections next.

Diffuse reflection

Figure 6 shows the estimated BRDF measurement (blue solid line) and reference (red solid line), for all the test samples at incidence angle -30º and reflection angle -10º. The mean NRMSD of these estimated spectra is 0.008. The BRDF estimation at diffuse reflection angles have low overall NRSMD, with minimum at 0.005 corresponding to sample 1 while the maximum is for sample 4 (Black, [100,100,100,0]). Similarly, ΔE_{00} and ΔE_{IPT} differences are low for these set of estimated spectra. ΔE_{IPT} of 0.01 is considered as a just noticeable difference (JND). The mean ΔE_{00} is lowest at 0.329 corresponding to sample 5 and mean ΔE_{00} is highest at 2.147 corresponding to sample 4. The mean ΔE_{IPT} is lowest at 0.004 corresponding to sample 5 and mean ΔE_{IPT} is highest at 0.016 corresponding to sample 4. The maximum ΔE_{IPT} is 0.072 corresponding to sample 11.

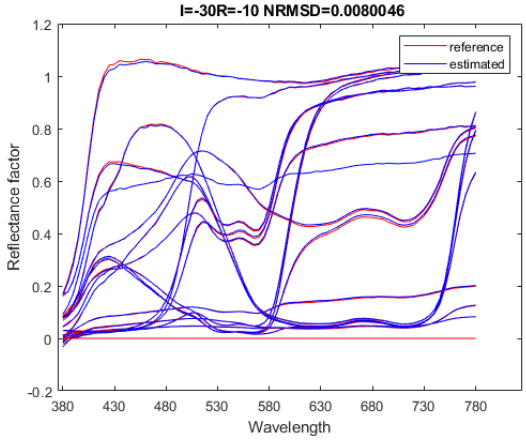

Figure 6. Estimated BRDF measurements plot of all the test samples at incidence angle -30º and reflection angle -10º with mean NRMSD of 0.008. Red solid line depicts reference measurement, and blue solid line depicts estimated measurement.

Specular reflection

Figure 7 shows the estimated BRDF measurement (blue solid line) and reference (red solid line), for all the test samples at incidence angle -30º and reflection angles 30º. The mean NRMSD of these estimated spectra is 0.104. There are only four specular reflections at angles (-60º, 60º), (-45º, 45º), (-30º,30º) and (-15º,15º) per sample. Two of these were used as predictors, and therefore only (-30º,30º) and (-15º,15º) specular reflectances have been estimated. The NRMSD is higher than NRMSD for diffuse reflections. Mean NRMSD is minimum at 0.029 corresponding to samples 3 and 13. The maximum is for sample 5 at 0.181. Similarly, ΔE_{00} and ΔE_{IPT} are comparatively high for these set of estimated spectra. The mean ΔE_{00} is lowest at 0.456 and mean ΔE_{IPT} is lowest at 0.012 corresponding to sample 13 and the mean ΔE_{00} is highest at 5.677 and mean ΔE_{IPT} is highest at 0.227 corresponding to sample 5. Maximum ΔE_{IPT} is 0.381 for sample 5.

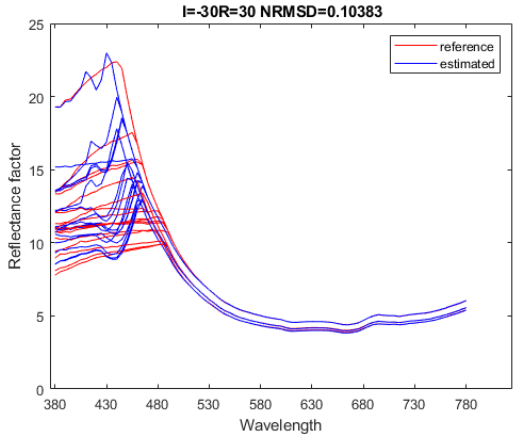

Figure 7. Estimated BRDF measurements plot of all the test samples at incidence angle -30º and reflection angle 30º with mean NRMSD of 0.104. Red solid line depicts reference measurement, and blue solid line depicts estimated measurement.

Near-to-specular reflection

Figure 8(a) shows an example of estimated BRDF measurement (blue solid line) and reference (red solid line), for test sample 5 at incidence angle -45º and reflection angle 50º and figure 8(b) shows the estimated BRDF measurement (blue solid line) and reference (red solid line), for test sample 5 at incidence angle -45º and reflection angle 55º. These spectra are reflectance factors of near-to-specular reflection i.e. reflection angle that is at most 10º away from specular reflection. This is specific to this BRDF dataset. The highest NRMSD and colour differences occur at these estimated spectra compared to the estimated spectra of diffuse reflection and specular reflection. Since, these are mixed reflections, the model is not able to fit properly using the base predictors. The mean NRMSD is lowest at 0.166 corresponding to sample 2. The maximum is for sample 7 at 0.947. The mean ΔE_{00} is lowest at 5.553 corresponding to sample 13 while mean ΔE_{IPT} is lowest at 0.062 corresponding sample 8. The mean ΔE_{00} is highest at 10.991 corresponding to smaple 6 and mean ΔE_{IPT} is highest at 0.148 corresponding to sample 7. Maxium ΔE_{IPT} is 0.484 corresponding to sample 7.

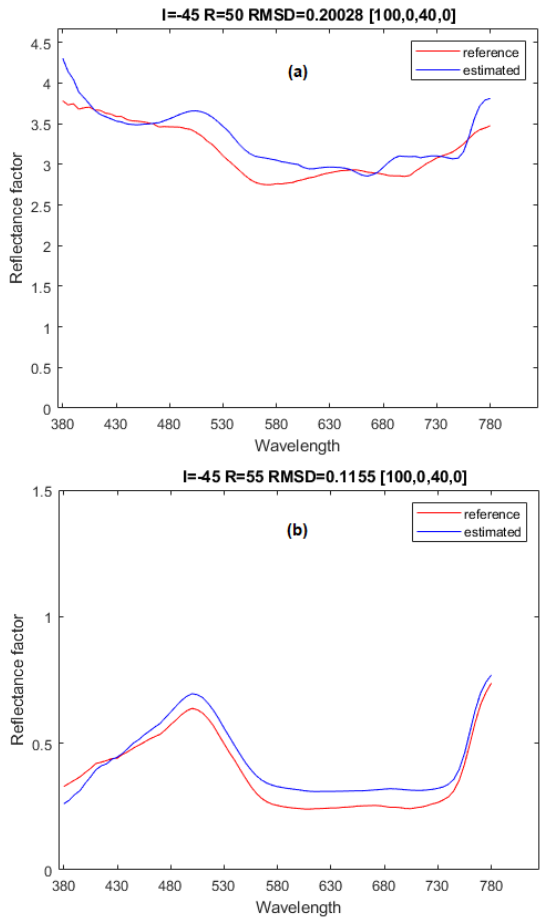

Figure 8. Estimated BRDF measurements plot of sample 5 at (a) incidence angle -45º and reflection angle 50º and (b) incidence angle -45º and reflection angle 55º. Red solid line depicts reference measurement, and blue solid line depicts estimated measurement.

Table1: Mean and max NRMSD of 13 test samples calculated category wise diffuse, specular, and near-to-specular.

Sr. No	Mean NRMSD Diffuse	Max NRMSD Diffuse	Mean NRMSD Specular	Max NRMSD Specular	Mean NRMSD Near Specular	Max NRMSD Near Specular
1	0.005	0.028	0.024	0.056	0.198	0.560
2	0.010	0.065	0.033	0.080	0.166	0.336
3	0.007	0.048	0.023	0.052	0.493	2.038
4	**0.134**	**0.924**	0.033	0.079	0.637	1.345
5	0.008	0.042	**0.117**	**0.198**	0.218	0.737
6	0.009	0.048	0.027	0.062	0.200	0.589
7	0.006	0.026	0.028	0.065	0.617	**3.003**
8	0.012	0.100	0.036	0.087	0.257	0.932
9	0.043	0.383	0.032	0.074	0.412	0.831
10	0.018	0.155	0.042	0.098	0.365	0.996
11	0.022	0.192	0.046	0.111	0.356	0.773
12	0.031	0.110	0.041	0.097	0.241	0.809
13	0.026	0.180	0.023	0.055	**0.790**	2.205

Table2: Mean and max ΔE_{00} of 13 test samples calculated category wise diffuse, specular, and near-to-specular.

Sr. No	Mean ΔE_{00} Diffuse	Max ΔE_{00} Diffuse	Mean ΔE_{00} Specular	Max ΔE_{00} Specular	Mean ΔE_{00} Near Specular	Max ΔE_{00} Near Specular
1	0.530	3.165	1.707	4.254	8.655	19.044
2	1.162	4.244	0.955	2.552	9.418	17.636
3	0.543	3.628	1.592	3.955	7.865	15.316
4	**2.147**	3.794	1.449	3.775	7.231	13.508
5	0.329	2.366	**5.677**	**9.974**	5.745	10.825
6	0.729	3.755	1.124	2.689	**10.991**	23.576
7	0.347	1.116	1.601	4.038	8.529	**24.996**
8	0.518	3.316	1.720	4.570	5.786	13.945
9	1.465	**5.675**	1.367	3.410	8.682	16.368
10	0.623	3.797	1.575	4.220	5.594	14.639
11	0.769	5.251	2.274	6.193	5.870	12.430
12	1.611	3.259	1.563	4.317	5.928	13.005
13	0.827	4.021	0.456	1.001	5.553	10.819

Table3: Mean and max ΔE_{IPT} of 13 test samples calculated category wise diffuse, specular, and near-to-specular.

Sr. No	Mean DEIPT Diffuse	Max DEIPT Diffuse	Mean DEIPT Specular	Max DEIPT Specular	Mean DEIPT Near Specular	Max DEIPT Near Specular
1	0.007	0.033	0.044	0.109	0.088	0.151
2	0.012	0.045	0.041	0.100	0.075	0.113
3	0.007	0.037	0.038	0.094	0.131	0.313
4	**0.016**	0.040	0.054	0.128	0.073	0.128
5	0.004	0.025	**0.227**	**0.381**	0.063	0.129
6	0.010	0.037	0.051	0.121	0.088	0.157
7	0.005	0.015	0.056	0.142	**0.148**	**0.484**
8	0.007	0.041	0.075	0.183	0.062	0.198
9	0.011	0.046	0.063	0.151	0.080	0.134
10	0.008	0.053	0.063	0.151	0.073	0.131
11	0.010	**0.072**	0.080	0.194	0.084	0.158
12	0.011	0.024	0.065	0.158	0.064	0.210
13	0.010	0.049	0.012	0.025	0.103	0.227

Luminance Comparison

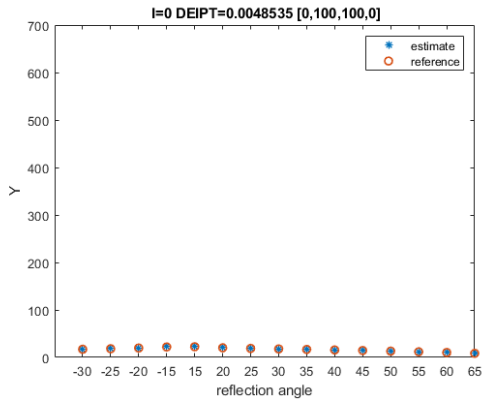

Figure 9. Luminance Y plot of test sample 3 at incidence angle 0º and reflection angles in x-axis, with mean ΔE_{IPT} of 0.0048. Red circle depicts reference Y, and blue asterisk depicts Y.

Figures 9-10 show luminance Y for sample 3 at incidence angles 0º, -15º, -30º, -45º and -60º respectively. Y value rises close to 700 at specular peaks. Y values are the worst predicted for reflection angles 5º and 10º away from specular peaks. For diffuse reflections the Y values are well predicted.

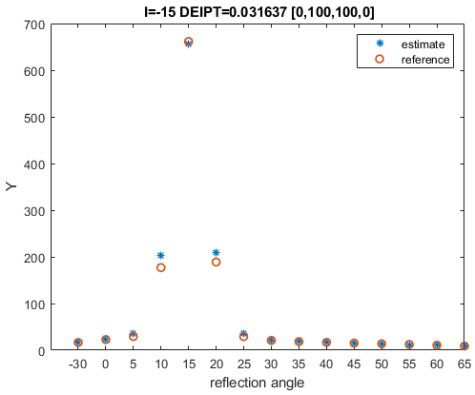

Figure 10. Luminance Y plot of test sample 3 at incidence angle -15º and reflection angles in x-axis, with mean ΔE_{IPT} of 0.0316. Red circle depicts reference Y, and blue asterisk depicts Y.

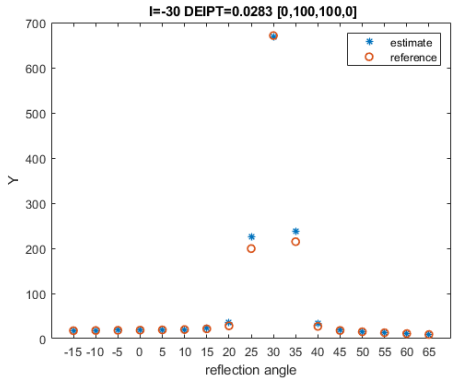

Figure 11. Luminance Y plot of test sample 3 at incidence angle -30º and reflection angles in x-axis, with mean ΔE_{IPT} of 0.0283. Red circle depicts reference Y, and blue asterisk depicts Y.

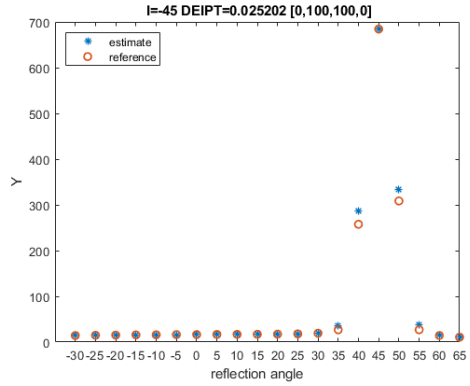

Figure 12. Luminance Y of test sample 3 at incidence angle -45º and reflection angles in x-axis, with mean ΔE_{IPT} of 0.0252. Red circle depicts reference Y, and blue asterisk depicts Y.

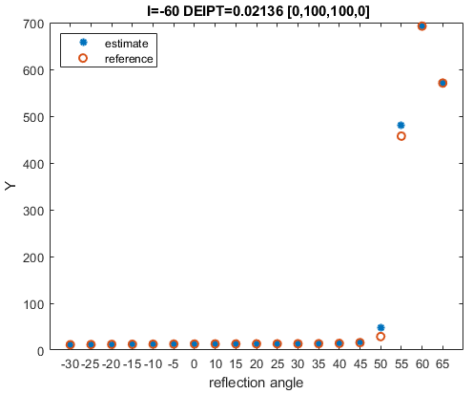

Figure 13. Luminance Y plot of test sample 3 at incidence angle -60º and reflection angles in x-axis, with mean ΔE_{IPT} of 0.0213. Red circle depicts reference Y, and blue asterisk depicts Y.

Visual representation

The reference and estimated BRDF measurements are converted to sRGB values, using which the reference sRGB and estimated sRGB images are created for visualisation purpose. Figure 14 shows that the diffuse part is quite accurately represented, when we compare the reference sRGB images to the estimated sRGB images. Large colour differences occur near-to-specular peak areas, and since the spectral shape is not properly estimated, visible hue differences are seen in near-to-specular angles. The luminance of the specular peak and at reflection angle of 5º around it is greater than that of the perfect diffuser, and therefore no colour difference can be represented as it is clipped to white in sRGB.

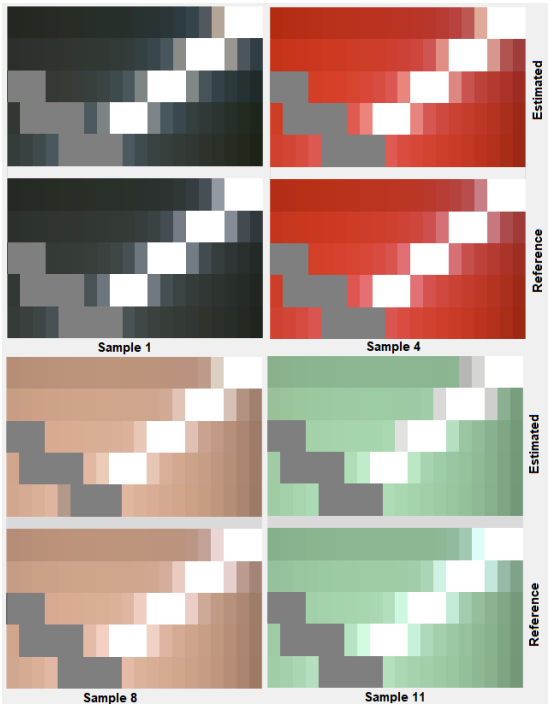

Figure 14. Visual representation of the BRDF measurements for samples 1,4,8 and 11. Reference and Estimated sRGB images are created using the measured BRDF and estimated BRDF respectively and representing them as patches in sRGB colour space for different incidence and reflection angles.

Conclusions

The results suggest that using polynomial regression and two predictors, spectra at diffuse reflection can be estimated well. Specular reflectances are overestimated but the relative distribution is reasonably well preserved. This model fails to estimate spectra at near-to-specular reflections, with reflection angles 5º and 10º from the specular peaks shows biggest error in this dataset. A different approach is needed to model these reflectances. The luminance Y values are well estimated for both diffuse and specular reflections. No colour sample has the overall best predicted results or the worst predicted, which suggests that mixing primaries to estimate spectra for other ink mixes works in this case. However, the worst prediction for diffuse spectra is for sample 1 i.e., black [100,100,100 0].

In the future, the specular and near-to-specular spectra should be modelled with a different approach such as a physically based BRDF model. Since printed substrates normally contain optical brightening agents, the fluorescent component of reflectance will need to be addressed. It will also be interesting to test BRDF datasets with different inks and substrates.

Acknowledgement

This project has received funding from the European Union's Horizon 2020 research and innovation programme under the Marie Skłodowska-Curie grant agreement No. 814158. Also, thanks to ApPEARS ESR 10 Donatela Saric from FOGRA for carrying out the reference measurements of all the samples.

References

[1] J. F. Murray-Coleman, and A.M. Smith. "The automated measurement of BRDFs and their application to luminaire modeling." Journal of the Illuminating Engineering Society, 19(1), pp.87-99 (1990).

[2] J.E. Proctor and P.Y. Barnes. "NIST high accuracy reference reflectometer-spectrophotometer." Journal of research of the National Institute of Standards and Technology, 101(5), p.619 (1990).

[3] J. Gu, C.I. Tu, R. Ramamoorthi, P. Belhumeur, W. Matusik and S. Nayar. "Time-varying surface appearance: acquisition, modeling and rendering". ACM Transactions on Graphics (TOG), 25(3), pp.762-771 (2006).

[4] M. Ben-Ezra, J. Wang, B. Wilburn, X. Li and L. Ma. An LED-only BRDF measurement device. In 2008 IEEE Conference on Computer Vision and Pattern Recognition (pp. 1-8). IEEE (2008).

[5] R. S. Marschner et al. "Image-based bidirectional reflectance distribution function measurement." Applied optics 39.16: 2592-2600 (2000).

[6] J. Günther, T. Chen, M. Goesele, I. Wald and H. P. Seidel. "Efficient acquisition and realistic rendering of car paint." In Vision, Modeling, and Visualization (Vol. 5, pp. 487-494). Akademische Verlagsgesellschaft Aka (2005).

[7] A. S. Sole, I. Farup and S. Tominaga. "An image-based multi-directional reflectance measurement setup for flexible objects." In Measuring, Modeling, and Reproducing Material Appearance 2015 (Vol. 9398, p. 93980J). International Society for Optics and Photonics (2015).

[8] A. S. Sole, I. Farup and P. Nussbaum. Evaluating an image based multi-angle measurement setup using different reflection models. Electronic Imaging, 2017(8), pp.101-107 (2017).

[9] T. Habib, P. Green and A. Sole. Implementing directional reflectance in a colour managed workflow. In London Imaging Meeting (Vol. 2020, No. 1, pp. 119-123). Society for Imaging Science and Technology (2020).

[10] T. Habib, P. Green and P. Nussbaum. BRDF rendering by interpolation of optimised model parameters. In Color and Imaging Conference (Vol. 2020, No. 28, pp. 162-168). Society for Imaging Science and Technology (2020).

[11] M.D. Fairchild, and P.H. Chen. Brightness, lightness, and specifying color in high-dynamic-range scenes and images. In Image Quality and System Performance VIII (Vol. 7867, p. 78670O). International Society for Optics and Photonics.

[12] T. Lu, F. Pu, P. Yin, T. Chen, W. Husak, J. Pytlarz, R. Atkins, J. Fr-hlich and G.M. Su, 2019. ITP colour space and its compression performance for high dynamic range and wide colour gamut video distribution. ZTE Communications, 14(1), pp.32-38.